

Reaction Mechanisms

A Palladium-Catalyzed Carbonylation Approach to Eight-Membered Lactam Derivatives with Antitumor Activity

Raffaella Mancuso,^{*,[a]} Dnyaneshwar S. Raut,^[a] Nadia Marino,^[b] Giorgio De Luca,^[c] Cinzia Giordano,^[d] Stefania Catalano,^[d] Ines Barone,^[d] Sebastiano Andò,^[d] and Bartolo Gabriele^{*,[a]}

Abstract: The reactivity of 2-(2-alkynylphenoxy)anilines under PdI₂/KI-catalyzed oxidative carbonylation conditions has been studied. Although a different reaction pathway could have been operating, N-palladation followed by CO insertion was the favored pathway with all substrates tested, including those containing an internal or terminal triple bond. This led to the formation of a carbamoylpalladium species, the fate of which, as predicted by theoretical calculations, strongly depended on the nature of the substituent on the triple bond. In particular, 8-endo-dig cyclization preferentially occurred when the triple bond was terminal, lead-

ing to the formation of carbonylated ζ-lactam derivatives, the structures of which have been confirmed by XRD analysis. These novel medium-sized heterocyclic compounds showed antitumor activity against both estrogen receptor-positive (MCF-7) and triple negative (MDA-MB-231) breast cancer cell lines. In particular, ζ-lactam **3j'** may represent a novel and promising antitumor agent because biological tests clearly demonstrate that this compound significantly reduces cell viability and motility in both MCF-7 and MDA-MB-231 breast cancer cell lines, without affecting normal breast epithelial cell viability.

Introduction

Medium-sized ring-based scaffolds (7–11-membered, carbonyl and heterocyclic) are molecular frameworks of particular interest, owing to their biological activity^[1] and occurrence in many important natural products.^[2] Despite their significance, relatively few efficient synthetic methods for their preparation through cyclization of acyclic precursors are known so far,^[3] compared with the quite abundant annulation protocols for the preparation of five- and six-membered rings. This is fundamentally due to a combination of unfavorable enthalpic (transannular interactions) and entropic (difficulty in closing a rela-

tively large ring) factors, which tend to raise the cyclization activation energy.^[4]

Catalytic cyclocarbonylation reactions are currently widely recognized as one of the most important and powerful synthetic tools for the direct preparation of cyclic carbonyl compounds from acyclic precursors.^[5,6] Although numerous examples are known in the literature for the formation of five-, six-, and even four-membered rings by cyclocarbonylation approaches, very few examples have been reported so far for the direct synthesis of medium-sized rings.^[5b,6] Considering our experience in oxidative carbonylation chemistry,^[5d,7] in particular, the use of the PdI₂/KI catalytic system we proposed some years ago for alkyne carbonylation,^[8] herein we have studied the reactivity of 2-(2-alkynylphenoxy)anilines under PdI₂/KI-catalyzed oxidative carbonylation conditions, with the aim of obtaining novel carbonylated medium-sized rings of biological interest.

Results and Discussion

In principle, different reaction pathways could be followed when 2-(2-alkynylphenoxy)anilines **1** are allowed to react in the presence of the PdI₂/KI catalytic system (leading in situ to K₂PdI₄) under oxidative carbonylation conditions (Scheme 1). The first possibility (path a) could correspond to N-palladation of **1**, with the formation of complex I, stabilized by triple-bond coordination, followed by CO insertion to give the carbamoylpalladium intermediate II. The latter species could then evolve either by direct attack from an external alcohol ROH, to afford acyclic carbamates **2** (path b), or through intramolecular *syn* 8-

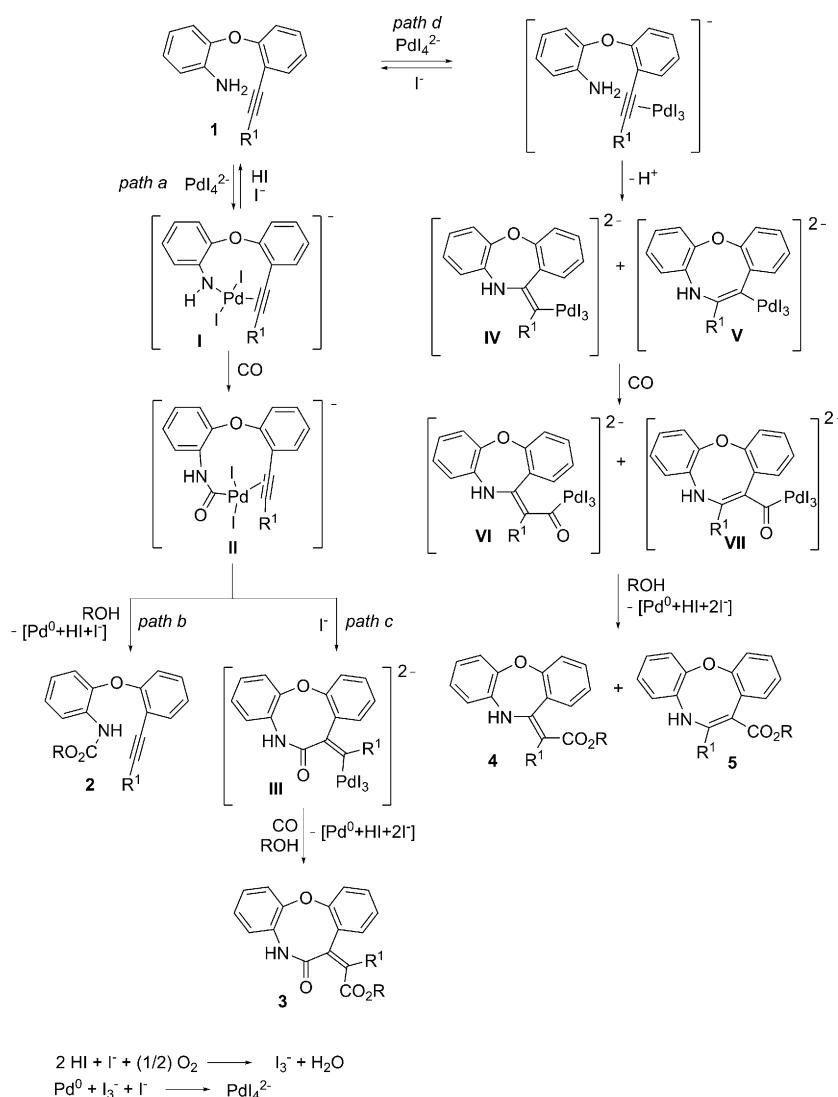
[a] Dr. R. Mancuso, Dr. D. S. Raut, Prof. Dr. B. Gabriele
Laboratory of Industrial and Synthetic Organic Chemistry (LISOC)
Department of Chemistry and Chemical Technologies
University of Calabria, Via Pietro Bucci, 12/C
87036 Arcavacata di Rende (CS) (Italy)
E-mail: raffaella.mancuso@unical.it
bartolo.gabriele@unical.it

[b] Dr. N. Marino
Department of Chemistry and Chemical Technologies
University of Calabria, Via Pietro Bucci, 14/C
87036 Arcavacata di Rende (CS) (Italy)

[c] Dr. G. De Luca
Institute on Membrane Technology, National Research Council
Via Pietro Bucci, 17/C, 87036 Arcavacata di Rende (CS) (Italy)

[d] Dr. C. Giordano, Prof. Dr. S. Catalano, Dr. I. Barone, Prof. Dr. S. Andò
Health Center and Department of Pharmacy
and Health and Nutritional Science
University of Calabria, 87036 Arcavacata di Rende (CS) (Italy)

Supporting information for this article is available on the WWW under <http://dx.doi.org/10.1002/chem.201504443>.



Scheme 1. Possible divergent pathways in the PdI₂/KI-catalyzed oxidative carbonylation of 2-(2-alkynylphenoxy)anilines **1**.

exo-dig triple-bond insertion to yield vinylpalladium intermediate **III**. Alkoxylation of the latter would eventually lead to the eight-membered lactam derivative **3** (path c). In both cases, the obtained Pd⁰ species would be reoxidized back to [PdI₄]²⁻ according to the mechanism we demonstrated several years ago,^[6] which involved oxidation of hydrogen iodide (also ensuing from the carbonylation process) to I₃⁻, followed by oxidative addition of the latter to Pd⁰ in the presence of iodide ligands. However, another possible reaction pathway could start with *anti*-intramolecular attack of the nucleophilic amino group to the triple bond coordinated to the metal center (path d; reactivity that we have observed in several other carbonylative heterocyclization reactions),^[5d] followed by alkoxy-carbonylation of the ensuing vinylpalladium complexes **IV** and/or **V**, finally leading to carbonylated heterocycles **4** and/or **5**. Clearly, from a conceptual and synthetic point of view, the most interesting process would correspond to the carbonylative ζ -lactamization route (path a followed by path c), leading to eight-membered lactams **3**, also considering the importance

of the ζ -lactam core, which is extensively found in natural and biologically relevant compounds.^[9]

To predict which pathway, of those shown in Scheme 1, was likely to be followed, starting from substrates **1**, we carried out theoretical calculations. Thus, a comparative analysis of the energies and geometries of the intermediates shown in Scheme 1 was carried out.^[10] First, optimization of the geometries of the isoelectronic reaction intermediates **III**, **VI**, and **VII** (with R¹ = CH₃, chosen as a simple model system for an internal triple bond) was carried out. All frequencies of these intermediates were positive, which indicated that they were minima in the respective reaction pathways. The energy difference between intermediates **III** and **VI** was +5.02 kcal mol⁻¹, whereas that between **III** and **VII** was -2.01 kcal mol⁻¹. These values indicate that paths a (leading to **III**) and d (leading to **VI** and/or **VII**) are equally probable. With reference to path d, intermediates **IV** and **V** (precursors of **VI** and **VII**, respectively) were also stable minima on the potential energy surface (PES). However, going towards the reactants, discrimination between paths a

and d could, in principle, still be at work, and could be related to different possible coordination modes of substrate **1** to the metal center. To prove this assumption, three structures (**A–C**) were built, representing the starting geometries for optimization (Figure 1). In particular, structure **A** differs from those of **B** and **C** in the palladium orientation with respect to the triple bond: in structure **A**, the metal center is close to the amino group, whereas in **B** and **C** palladium is coordinated from the opposite position with respect to the $-\text{NH}_2$ group. In turn, structure **B** differs from that of **C** in the $-\text{NH}_2$ orientation with respect to the triple bond, in particular, in **B**, $\text{NH}\cdots\pi$ (orbitals) hydrogen bonding is present.^[11]

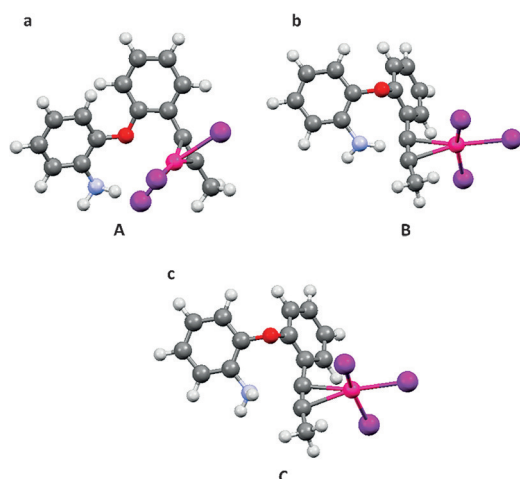


Figure 1. Possible coordination modes of substrate **1** ($R^1 = \text{Me}$) to the metal center: starting geometries **A** (a), **B** (b), and **C** (c) used for geometry optimization (pink: Pd; violet: I; red: O, gray: C; white: H).

All optimized structures obtained from these initial geometries showed positive frequencies, which demonstrated that they were minima. The optimized geometries for structures **A** and **B**, labeled **A'** and **B'**, are shown in Figure 2.

These structures appear to be stabilized by an intramolecular hydrogen bond ($\text{NH}\cdots\text{I}$, 2.9 Å), involving an iodine atom and a hydrogen atom on the amino group (Figure 2a and b). The energy difference between **B'** and **A'** was only $-3.43 \text{ kcal mol}^{-1}$, which suggested that two minima were in equilibrium. Comparing **A'** (Figure 2a) with the non-optimized structure **A** (Figure 1a), it can be seen that the catalyst orientation does not change significantly from the initial (**A**) to the optimized (**A'**) structure. In **A'**, the $\text{N}\cdots\text{Pd}$ and $\text{N}\cdots\text{C}$ distances (in which C is the carbon of the triple bond closest to nitrogen) were 4.4 and 4.9 Å, respectively. This suggests that **A'** should preferentially evolve through the formation of a N–Pd bond, leading to intermediate **I**, rather than through that of a N–C bond, which would lead to intermediate **IV**. On the other hand, comparing the optimized structure **B'** (Figure 2b) with the initial structure **B** (Figure 1b), it can be observed that the $\text{NH}\cdots\pi$ hydrogen bond in the initial geometry **B** is broken down after geometry optimization, in favor of a more stable $\text{NH}\cdots\text{I}$ noncovalent bond, with simultaneous rotation of the catalyst from its initial

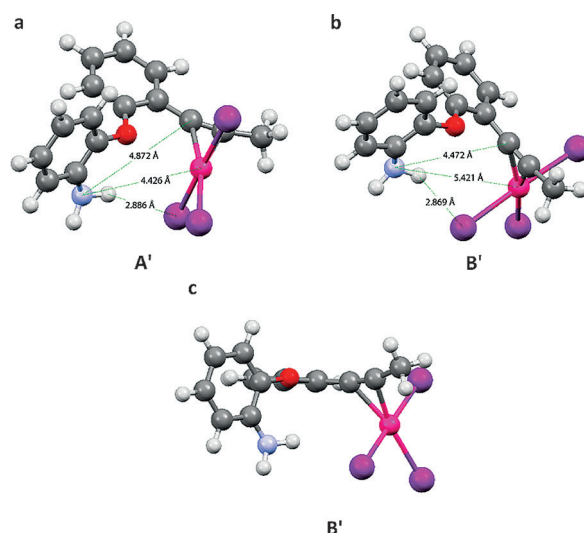


Figure 2. Optimized geometries for structures **A** and **B**, labeled **A'** (a) and **B'** (b, c), respectively (pink: Pd; violet: I; red: O, gray: C; white: H).

position. The displacement of the $\text{PdI}_3\cdots\pi$ moiety from its initial geometry is caused by a marked rotation of the Ph–O–Ph dihedral angle, as shown in Figure 2c. Key distances in **B'**, as those given for **A'**, are 5.4 Å ($\text{N}\cdots\text{Pd}$ bond) and 4.5 Å ($\text{N}\cdots\text{C}$ bond), respectively (Figure 2b). However, the formation of a N–C bond, leading to intermediate **IV**, would imply an unfavorable movement of the $-\text{NH}_2$ group toward the position shown in the nonoptimized structure **B** (Figure 1b), with an inverse rotation of Ph–O–Ph dihedral angle. With regard to starting geometry **C**, shown in Figure 1c, a marked rotation of the dihedral angle Ph–O–Ph was always obtained after optimization; again, this rotation arranged the phenyl rings perpendicularly, with the $-\text{NH}_2$ farther away from the triple bond with respect to the starting geometry.

Therefore, this computational analysis suggests that path a, via intermediate **I**, should be favored with respect to path d, via intermediates **IV/V** (Scheme 1), and, as a result, products **2** and/or **3** (ensuing from path a) are predicted to be formed preferentially over products **4** and/or **5** (derived from path d). It is important to emphasize that the geometry of intermediate **I** was also optimized, and its existence as a stable minimum on the PES was confirmed; the optimized structure is shown in Figure 3.

According to path a (Scheme 1), CO insertion in the N–Pd bond of intermediate **I** would lead to carbamoylpalladium intermediate **II**, which, in turn, could follow either path b (from external nucleophilic displacement by ROH, to give acyclic carbamates **2**) or path c (from intramolecular triple bond insertion into the C–Pd bond, to give intermediate **III**, followed by alkoxycarbonylation, eventually leading to ζ -lactams **3**). The latter pathway was expected to be less favored in the case of an internal triple bond ($R^1 \neq \text{H}$), as usually observed in other $[\text{PdI}_4]^{2-}$ -catalyzed heterocyclocarbonylation processes,^[5d] for steric reasons. Thus, to predict which product could be formed preferentially between **2** (ensuing from path b) or **3** (ensuing from path c), depending on the nature of the triple bond (in-

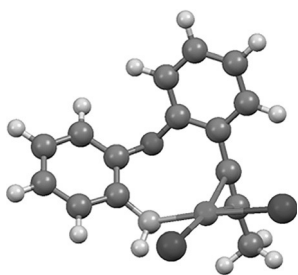


Figure 3. Optimized geometry for intermediate I ($R^1 = \text{CH}_3$).

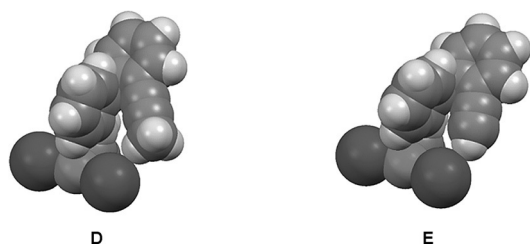


Figure 4. Optimized geometries for intermediate II with $R^1 = \text{Me}$ (D) and H (E).

ternal or external), the geometries of intermediates II with both $R^1 = \text{CH}_3$ (D) and $R^1 = \text{H}$ (E) were optimized (Figure 4).

As seen from Figure 4, in D ($R^1 = \text{Me}$) the C...C distance between the carbon of the carbonyl and the carbon of the triple bond is 5.1 Å, and the H₂CH...I distance is 3.1 Å, whereas in E ($R^1 = \text{H}$) both the C...C and H...I distances are appreciably shorter (4.6 and 2.9 Å, respectively). This finding indeed suggests that the cyclocarbonylation pathway (path c) may be favored with an external triple bond ($R^1 = \text{H}$), whereas, in the case of an internal triple bond ($R^1 = \text{Me}$), this route may be significantly more difficult, since the key distances are systematically longer owing to steric hindrance exerted by the R^1 substituent. To further confirm this supposition, the geometries of intermediates III with both $R^1 = \text{CH}_3$ (F) and H (G) were also optimized (Figure 5). For both F and G, the Hessian showed positive eigenvalues. Once again, they were minima on the PES, and therefore, they were both possible. The energy differences between structures F and G and intermediates D and E, respectively, were then calculated to support the hypothesis that the formation of III was favored when $R^1 = \text{H}$. From a thermody-

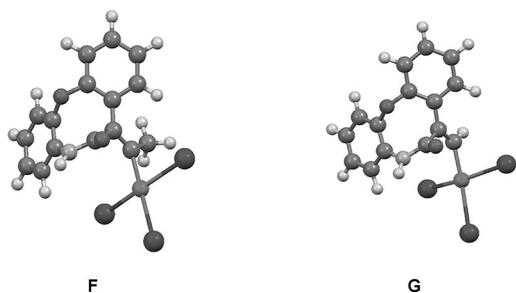
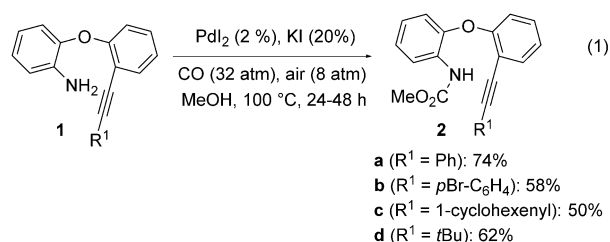


Figure 5. Optimized geometries for intermediate III with $R^1 = \text{Me}$ (F) and H (G).

amic point of view, the difference in energy between intermediates III and II yields information on the relative stability of these structures in equilibrium between them. The energy gap between intermediates G and E ($R^1 = \text{H}$) was 8.24 kcal mol⁻¹ larger than the corresponding energy difference between F and D ($R^1 = \text{CH}_3$). This means that the stability of intermediate III with respect to II is greater when $R^1 = \text{H}$; thus confirming that the formation of III is more favored when $R^1 = \text{H}$.

Thus, the results obtained by the theoretical calculations can be summarized as follows: 1) Both paths a and d, leading to intermediates II and VI and/or VII, respectively, can, in principle, be followed. 2) Path a is expected to be more favored with respect to path d. 3) Path c, derived from path a and leading to the desired ζ -lactam derivative 3 through the formation of carbamoylpalladium complex II, is more likely to be followed when $R^1 = \text{H}$, otherwise path b, leading to acyclic carbamate 2, is more favored. This may be ascribed to the steric effect exerted by the R^1 substituent on the triple bond, which hinders its insertion into the carbamoylpalladium bond when $R^1 \neq \text{H}$.

To verify these hypotheses, we began to investigate the reactivity of a substrate containing an internal triple bond, such as 2-[2-(2-phenylethynyl)phenoxy]aniline (**1a**; $R^1 = \text{Ph}$). This substrate was allowed to react with CO, O₂, and MeOH ($R = \text{Me}$), which was also used as the solvent (substrate concentration = 0.05 mmol of **1** per mL of MeOH), at 100 °C and under 40 atm (at 25 °C) of a 4:1 mixture of CO/air, in the presence of catalytic amounts of PdI₂ (2 mol%) in conjunction with KI (KI/PdI₂ molar ratio = 10). After 24 h, carbamate **2a** was isolated in 74% yield [Eq. (1)]. Similar results were obtained with other substrates, containing *p*-bromophenyl, alkenyl, or alkyl substituents on the triple bond; the corresponding acyclic carbamates were formed in 50–62% yield after 24–48 h [Eq. (1)]. The structure of **2b** ($R^1 = p\text{-Br-C}_6\text{H}_4$) was confirmed by XRD analysis (see the Supporting Information for details), and unidentified heavy products (chromatographically immobile materials) accounted for the remaining part of the converted substrates.



Thus, the results obtained with substrates containing an internal triple bond showed that, in agreement with theoretical predictions, path a was preferentially followed with respect to path d, and then path b was favored over path c, eventually leading to acyclic carbamates 2. On the other hand, as seen above, theoretical calculations also predicted that intermediate II (from path a) could follow path c when the triple bond was terminal ($R^1 = \text{H}$). Accordingly, we next turned our attention to the reactivity of substrates containing a terminal triple bond. The first experiments were carried out with 2-(2-ethynylphe-

noxy)aniline (**1e**), which was allowed to react under conditions similar to those employed previously for substrates **1a–d**. Gratifyingly, after 15 h, ζ -lactam **3e** was isolated in 63% yield (Table 1, entry 1); thus confirming the validity of our hypotheses. This result was noteworthy when considering the possible competitive pathways that could have been at work (Scheme 1), the importance of realizing a novel ζ -lactamization process by a direct carbonylative approach, and the potential importance of the product obtained for various applications. The reaction was repeated in EtOH and a slightly higher yield of the corresponding ethyl ester **3e'** was obtained (71%, Table 1, entry 2). The structure of **3e'** was confirmed by XRD analysis (see the Supporting Information for details), and the *Z* stereochemistry around the double bond was in perfect agreement with the mechanism shown in Scheme 1, path c. The next experiments, carried out with differently substituted substrates, confirmed the formation of the corresponding eight-membered lactams **3f–i** and **3f'–k'** in satisfactory yields in all cases (53–75%; Table 1, entries 3–12).

Considering the bioactivity reported in the literature for eight-membered lactam systems, we tested the newly synthesized ζ -lactams for their biological activity as antitumor agents against different breast cancer cell lines. To this aim, we evaluated the effects of increasing concentrations (1, 10, 25, 50, 75, and 100 μM) of ζ -lactams for 96 h on cell viability in estrogen receptor (ER)-positive MCF-7 and ER-negative, progesterone receptor (PR)-negative, and human epidermal growth factor receptor 2 (HER2)-negative MDA-MB-231 human breast cancer cells by using 3-(4,5-dimethylthiazol-2-yl)-2,5-diphenyltetrazolium bromide (MTT) assays. Although almost all tested compounds induced a decrease in breast cancer cells viability (data not shown), ζ -lactam **3j'** was the most active in reducing anchorage-dependent growth of breast cancer cells (Figure 6). In particular, as shown in Figure 6A, treatment for 96 h with **3j'** induced a significant decrease in cell viability in MCF-7 (Figure 6A, top) and in MDA-MB-231 cells (Figure 6A, middle).

The half-maximal inhibitory concentration (IC_{50}) values of ζ -lactam **3j'** for the cell lines tested are shown in Table 2. Notably, treatment with ζ -lactam **3j'** at doses of IC_{50} values calculated in our breast cancer models did not elicit any noticeable effects in MCF-10A nonmalignant breast epithelial cell viability (Figure 6A, bottom). The ability of **3j'** to inhibit cell growth was also evaluated by using anchorage-independent growth assays (soft-agar assay), which better reflected in vivo three-dimensional tumor growth. MCF-7 and MDA-MB-231 cells were plated in soft agar and then treated with ζ -lactam **3j'** (50 μM) for 14 days. At the end of treatment, colo-

Table 1. Synthesis of alkyl (*Z*)-(6-oxo-5,6-dihydro-12-oxa-5-azabenzocycloocten-7-ylidene)acetates **3e–i** and **3e'–k'** by PdI₂/KI-catalyzed oxidative cyclocarbonylation-alkoxycarbonylation of 2-(2-ethynylphenoxy)anilines **1e–k**.^[a]

Entry	1	R	t [h]	3	Yield [%] ^[b]
1		Me	15		63
2	1e	Et	24		71
3		Me	15		72
4	1f	Et	24		70
5		Me	15		62
6	1g	Et	24		75
7		Me	15		73
8	1h	Et	24		69
9		Me	15		72
10	1i	Et	24		63

Table 1. (Continued)

Entry	1	R	t [h]	3	Yield [%] ^[b]
11		Et	24		74
12		Et	24		53

[a] All reactions were carried out at 100 °C in ROH as the solvent (0.05 mmol of **1** per mL of solvent) under 40 atm of a 4:1 mixture of CO/air (at 25 °C) in the presence of PdI₂ (2 mol%) in conjunction with KI (20 mol%). [b] Yield of product isolated based on starting material **1**.

Table 2. IC₅₀ values of **3j'** for MDA-MB 231 and MCF-7 cells on anchorage-dependent growth.

Cell lines	IC ₅₀ [μM]	95% confidence interval
MDA-MB 231	27.34	20.37–36.69
MCF-7	21.29	11.96–37.89

nies of > 50 μm in diameter were counted. As shown in Figure 6B, treatment with **3j'** significantly inhibited anchorage-independent growth of both MCF-7 and MDA-MB-231 cells. We then examined the ability of **3j'** to inhibit cell movement in wound-healing scratch assays (Figure 6C). During 24 h of observation, MCF-7 and MDA-MB-231 cells moved in either direction to close the gap, although treatment with **3j'** strongly reduced breast cancer cell movement. Taken together, these data clearly indicate that the new ζ-lactam derivative **3j'** is able to inhibit breast cancer cell proliferation and motility, without affecting normal breast epithelial cell viability.

Conclusion

We found that readily available 2-(2-ethynylphenoxy)anilines **1**, containing a terminal triple bond (R¹=H), could be directly converted into a novel class of medium-sized heterocyclic derivatives **3**, through a new PdI₂/KI-catalyzed carbonylative ζ-lactamization–alkoxycarbonylation process. In agreement with theoretical calculations, the process started with N-palladation of **1**, followed by CO insertion, intramolecular triple bond insertion, and alkoxycarbonylation. The formation of ζ-lactams **3** from simple building blocks (**1**, CO, ROH, and O₂) in a multi-component manner represents a significant achievement, also

in view of the biological relevance of these compounds. Biological tests showed that the newly synthesized ζ-lactam **3j'** exerted antiproliferative effects on different breast cancer cell lines, without affecting normal breast epithelial cell viability. Other studies are currently ongoing to elucidate its biochemical mechanism of action, and will be reported in due course.

Experimental Section

General

Melting points are uncorrected. ¹H and ¹³C NMR spectra were recorded on a Bruker DPX Avance 300 spectrometer at 25 °C in CDCl₃ at 300 or 500 MHz, and 75 or 126 MHz, respectively, with Me₄Si as an internal standard. ¹⁹F NMR spectra were recorded on a Bruker DPX Avance 500 spectrometer at 25 °C in CDCl₃ or [D₆]DMSO at 471 MHz with CFCl₃ as an internal standard. Chemical shifts (δ) and coupling constants (*J*) are given in ppm and Hz, respectively. IR spectra were recorded on a JASCO FTIR 4200 spectrometer. GC-MS spectra were recorded on a Shimadzu QP-2010 GC-MS apparatus at an ionization voltage of 70 eV. Microanalyses were carried out with a Thermo-Fischer Elemental Analyzer Flash 2000 instrument. All reactions were analyzed by TLC on silica gel 60 F₂₅₄ or on neutral alumina (Merck) and by gas liquid chromatography (GLC) with a gas chromatograph equipped with capillary columns with polymethylsilicone and 5% phenylsilicone as the stationary phase. Column chromatography was performed on silica gel 60. Evaporation refers to the removal of solvent under reduced pressure.

Preparation of substrates **1**

2-(2-Alkynylphenoxy)anilines were prepared by coupling between the corresponding 2-(2-iodophenoxy)anilines^[12] and a suitable terminal alkyne, followed (in the case of the reaction with trimethylsilylacetylene) by deprotection, as described below. All other materials were commercially available and were used without further purification.

General procedure for the preparation of **1 a–d** and 2-(2-trimethylsilyl)ethynylphenoxy)anilines

Under nitrogen and with stirring, anhydrous Et₃N (330 mg, 3.3 mmol), [PdCl₂(PPh₃)₂] (12.8 mg, 3.2 × 10⁻² mmol), CuI (30.4 mg, 0.16 mmol), and the 1-alkyne [2.4 mmol; phenylacetylene, 245 mg; *p*-bromophenylacetylene, 434 mg; 1-ethynylcyclohex-1-ene, 255 mg; *tert*-butylacetylene, 200 mg; trimethylsilylacetylene, 235 mg] were added in this order to a solution of the 2-(2-iodophenoxy)aniline [1.6 mmol; 2-(2-iodophenoxy)aniline, 498 mg; 2-(2-iodophenoxy)-5-methylaniline, 520 mg; 2-(2-iodophenoxy)-5-methoxyaniline, 546 mg; 1-[3-amino-4-(2-iodophenoxy)phenyl]ethanone, 565 mg; methyl 3-amino-4-(2-iodophenoxy)benzoate, 591 mg; 2-(2-iodophenoxy)-5-cyanoaniline, 538 mg; 2-(2-iodophenoxy)-5-trifluoromethylaniline, 607 mg] in anhydrous THF (5 mL). The resulting mixture was allowed to stir at room temperature for 8 h (for *p*-bromophenylacetylene, *tert*-butylacetylene, and trimethylsilylacetylene) or at 40 °C for 15 h (for 1-ethynylcyclohex-1-ene). After cooling to room temperature, a saturated aqueous solution of NH₄Cl was added (10 mL), and the mixture was extracted with

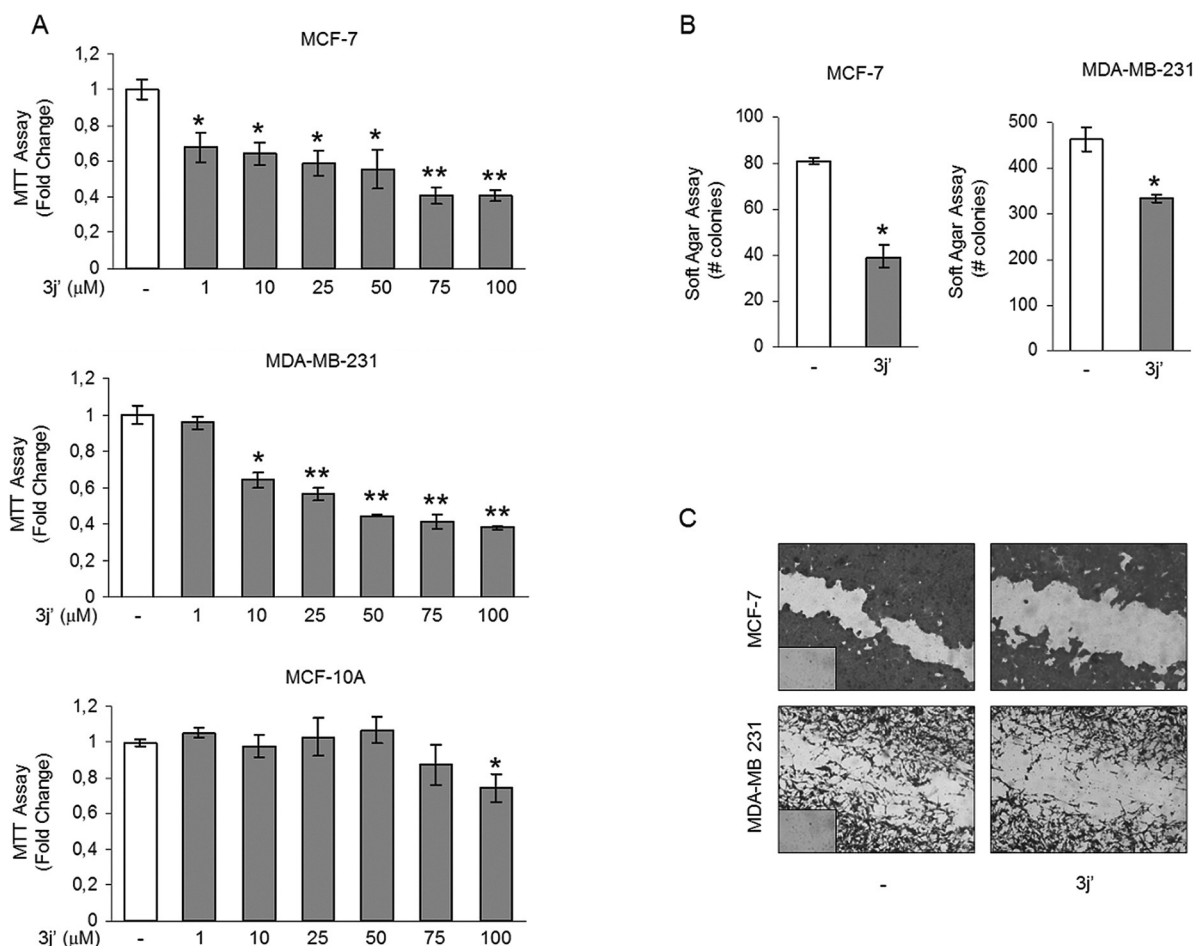


Figure 6. The ζ -lactam derivative **3j'** inhibits breast cancer cell growth. A) MTT assays in MCF-7, MDA-MB-231, and MCF-10A cells treated with vehicle (-) or increasing concentrations (1, 10, 25, 50, 75, and 100 μM) of **3j'** for 96 h. Cell proliferation is expressed as fold change versus control (vehicle-treated cells). The values represent the means \pm standard deviation (SD) of three different experiments, each performed with triplicate samples. B) Soft-agar growth assay in MCF-7 and MDA-MB-231 cells plated in 0.35% agarose and treated with ζ -lactam **3j'** (50 μM). After 14 days of growth, colonies of $> 50 \mu\text{m}$ diameter were counted. Data are the mean colony number \pm SD of three plates and representative of two independent experiments. C) Cells were subjected to wound-healing scratch assays with images captured at 0 and 24 h after incubation with vehicle (-) or **3j'** (50 μM) by using phase-contrast microscopy. Small squares, time=0. * $P < 0.05$ and ** $P < 0.001$ compared with vehicle-treated cells.

AcOEt (3 \times 15 mL). The collected organic layers were washed with brine (40 mL) and dried over Na_2SO_4 . After filtration and evaporation of the solvent, the residue was purified by column chromatography on silica gel as the stationary phase with 7:3 hexane/AcOEt as the eluent to give pure **1a-d** and 2-(2-trimethylsilylanylethynylphenoxy)anilines. 2-(2-Phenylethynylphenoxy)aniline (**1a**), yellow solid, 365 mg, 80%; 2-[2-(4-bromophenylethynyl)phenoxy]aniline (**1b**), yellow solid, 466 mg, 80%; 2-(2-cyclohex-1-eynylethynylphenoxy)aniline (**1c**), yellow oil, 375 mg, 81%; 2-[2-(3,3-dimethylbut-1-ynylphenoxy)aniline (**1d**), yellow solid, 344 mg, 81%; 2-(2-trimethylsilylanylethynylphenoxy)aniline, gray solid, 342 mg, 76%; 5-methyl-2-(2-trimethylsilylanylethynylphenoxy)aniline, yellow solid, 340 mg, 72%; 5-methoxy-2-(2-trimethylsilylanylethynylphenoxy)aniline, brown oil, 419 mg, 84%; 1-[3-amino-4-(2-trimethylsilylanylethynylphenoxy)phenyl]ethanone, brown solid, 440 mg, 85%; methyl 3-amino-4-(2-trimethylsilylanylethynylphenoxy)benzoate, yellow solid, 478 mg, 88%; 3-amino-4-(2-trimethylsilylanylethynylphenoxy)benzotrile, white solid, 358 mg, 88%; 5-trifluoromethyl-2-(2-trimethylsilylanylethynylphenoxy)aniline, yellow solid, 458 mg, 82%.

Deprotection of 2-[2-(trimethylsilylethynyl)phenoxy]anilines to give **1e-k**

With stirring and under nitrogen, K_2CO_3 (622 mg, 4.5 mmol) was added to a solution of the 2-[2-(trimethylsilylethynyl)phenoxy]aniline obtained as described above [1.5 mmol; 2-(2-trimethylsilylanylethynylphenoxy)aniline, 422 mg; 5-methyl-2-(2-trimethylsilylanylethynylphenoxy)aniline, 443 mg; 5-methoxy-2-(2-trimethylsilylanylethynylphenoxy)aniline, 467 mg; 1-[3-amino-4-(2-trimethylsilylanylethynylphenoxy)phenyl]ethanone, 485 mg; methyl 3-amino-4-(2-trimethylsilylanylethynylphenoxy)benzoate, 509 mg; 3-amino-4-(2-trimethylsilylanylethynylphenoxy)benzotrile, 460 mg; 5-trifluoromethyl-2-(2-trimethylsilylanylethynylphenoxy)aniline, 524 mg] in anhydrous methanol (5 mL). The resulting mixture was allowed to stir at room temperature for 3 h, and then it was filtered through Celite to remove K_2CO_3 , followed by washing with MeOH (50 mL). The resulting filtrate was evaporated to dryness to give the crude product, which was dissolved in CH_2Cl_2 (40 mL) and washed with brine (50 mL) and water (50 mL). After drying over Na_2SO_4 and

evaporation of the solvent, the residue was purified by column chromatography on silica gel by using hexane/AcOEt from 95:5 to 7:3 as the eluent to give pure **1e–k**. 2-(2-Ethynylphenoxy)aniline (**1e**), white solid, 245 mg, 78%; 5-methyl-2-(2-ethynylphenoxy)aniline (**1f**), yellow oil, 255 mg, 76%; 5-methoxy-2-(2-ethynylphenoxy)aniline (**1g**), yellow solid, 302 mg, 84%; 1-[3-amino-4-(2-ethynylphenoxy)phenyl]ethanone (**1h**), yellow solid, 305 mg, 81%; methyl 3-amino-4-(2-ethynylphenoxy)benzoate (**1i**), yellow solid, 337 mg, 84%; 3-amino-4-(2-ethynylphenoxy)benzonitrile (**1j**), white solid, 257 mg, 72%; 2-(2-ethynylphenoxy)-5-trifluoromethylaniline (**1k**), yellow oil, 362 mg, 87%.

Compound 1a: Yellow solid, m.p. 119–120 °C; IR (KBr): $\tilde{\nu}$ = 3473 (m, br), 3384 (m, br), 3057 (m), 2215 (vw), 1619 (m), 1500 (s), 1447 (m), 1266 (m), 1221 (s), 1188 (w), 1099 (m), 889 (w), 753 (s), 691 cm^{-1} (m); $^1\text{H NMR}$ (300 MHz, CDCl_3): δ = 7.63–7.39 (m, 3H; aromatic), 7.39–7.17 (m, 4H; aromatic), 7.12–6.64 (m, 6H; aromatic), 3.87 ppm (brs, 2H; NH_2); $^{13}\text{C NMR}$ (75 MHz, CDCl_3): δ = 157.8, 143.6, 138.5, 133.6, 131.7, 129.7, 128.3, 124.8, 123.4, 122.9, 119.7, 118.6, 117.2, 116.4, 114.7, 94.3, 85.2 ppm; GC-MS: m/z (%): 285 (100) [M^+], 268 (29), 256 (29), 244 (66), 230 (5), 215 (12), 183 (78), 176 (14), 165 (21), 150 (9), 127 (12), 80 (20); elemental analysis calcd (%) for $\text{C}_{20}\text{H}_{15}\text{NO}$ (285.34): C 84.19, H 5.30, N 4.91; found: C 84.21, H 5.29, N 4.92.

Compound 1b: Yellow solid, m.p. 67–68 °C; IR (KBr): $\tilde{\nu}$ = 3466 (m, br), 3379 (m, br), 2218 (vw), 1619 (m), 1500 (s), 1478 (m), 1446 (w), 1264 (w), 1221 (s), 1187 (w), 1069 (w), 1010 (m), 823 (m), 747 cm^{-1} (s); $^1\text{H NMR}$ (300 MHz, CDCl_3): δ = 7.58–7.51 (m, 1H; aromatic), 7.47–7.38 (m, 2H; aromatic), 7.34–7.26 (m, 2H; aromatic), 7.26–7.21 (m, 1H; aromatic), 7.10–7.02 (m, 1H; aromatic), 7.02–6.93 (m, 1H; aromatic), 6.91–6.82 (m, 3H; aromatic), 6.75–6.67 (m, 1H; aromatic), 3.76 ppm (brs, 2H; NH_2); $^{13}\text{C NMR}$ (75 MHz, CDCl_3): δ = 157.7, 143.5, 138.3, 133.5, 133.1, 131.5, 130.0, 124.8, 122.9, 122.5, 122.3, 119.6, 118.7, 117.2, 116.4, 114.3, 93.2, 86.3 ppm; GC-MS: m/z (%): 365 (51) [$M+2^+$], 363 (51) [M^+], 324 (36), 322 (36), 283 (65), 268 (18), 254 (27), 239 (10), 215 (9), 183 (100), 176 (18), 163 (15), 150 (12), 142 (30), 127 (22), 113 (8), 80 (20); elemental analysis calcd (%) for $\text{C}_{20}\text{H}_{14}\text{BrNO}$ (364.24): C 65.95, H 3.87, Br 21.94, N 3.85; found: C 65.99, H 3.86, Br 21.96, N 3.86.

Compound 1c: Yellow oil; IR (film): $\tilde{\nu}$ = 3468 (m, br), 3381 (m, br), 2930 (m), 2204 (w), 1619 (m), 1501 (s), 1483 (s), 1446 (m), 1267 (w), 1218 (s), 748 (s) cm^{-1} ; $^1\text{H NMR}$ (300 MHz, CDCl_3): δ = 7.45 (dd, J = 7.6, 1.6 Hz, 1H; aromatic), 7.22–7.14 (m, 1H; aromatic), 7.05–6.92 (m, 2H; aromatic), 6.89–6.78 (m, 3H; aromatic), 6.75–6.66 (m, 1H; aromatic), 6.19–6.11 (m, 1H; =CH), 3.86 (brs, 2H; NH_2), 2.22–2.06 (m, 4H; cyclohexenyl ring), 1.70–1.52 ppm (m, 4H; cyclohexenyl ring); $^{13}\text{C NMR}$ (75 MHz, CDCl_3): δ = 157.5, 143.6, 139.8, 138.5, 135.3, 133.4, 129.1, 124.7, 122.8, 119.8, 118.6, 117.0, 116.4, 96.2, 82.4, 29.1, 25.8, 22.4, 21.5 ppm; GC-MS: m/z (%): 289 (100) [M^+], 272 (14), 260 (47), 246 (95), 233 (27), 220 (27), 205 (16), 183 (78), 165 (19), 152 (16), 139 (8), 115 (14), 102 (7), 80 (20), 65 (12); elemental analysis calcd (%) for $\text{C}_{20}\text{H}_{19}\text{NO}$ (289.37): C 83.01, H 6.62, N 4.84; found: C 83.04, H 6.60, N 4.83.

Compound 1d: Pale yellow solid, m.p. 75–76 °C; IR (KBr): $\tilde{\nu}$ = 3384 (w, br), 3348 (m, br), 2969 (m), 2231 (vw), 1620 (s), 1485 (m), 1265 (m), 745 cm^{-1} (vs); $^1\text{H NMR}$ (300 MHz, CDCl_3): δ = 7.42 (dd, J = 7.8, 1.6 Hz, 1H; aromatic), 7.24–7.16 (m, 1H; aromatic), 7.07–6.99 (m, 1H; aromatic), 6.98–6.88 (m, 2H; aromatic), 6.83–6.74 (m, 2H; aromatic), 6.72–6.64 (m, 1H; aromatic), 3.90 (brs, 2H; NH_2), 1.22 ppm (s, 9H; tBu); $^{13}\text{C NMR}$ (75 MHz, CDCl_3): δ = 157.2, 144.1, 138.0, 133.4, 128.8, 124.1, 123.0, 118.5, 118.2, 117.9, 116.1, 115.8, 103.8, 74.6, 30.8, 28.0 ppm; GC-MS: m/z (%): 265 (100), 250 (98), 234 (37), 220 (62), 209 (48), 208 (69), 183 (55), 180 (27), 157 (14), 141 (13), 128 (15), 115 (22), 102 (8), 91 (11), 80 (17), 65 (15); elemental analysis

calcd (%) for $\text{C}_{18}\text{H}_{19}\text{NO}$ (265.35): C 81.47, H 7.22, N 5.28; found: C 81.51, H 7.20, N 5.29.

Compound 1e: Colorless solid, m.p. 64–65 °C; IR (KBr): $\tilde{\nu}$ = 3464 (w, br), 3377 (m, br), 3281 (m, br), 2107 (vw), 1620 (m), 1500 (s), 1482 (s), 1443 (m), 1270 (m), 1231 (s), 1192 (m), 886 (w), 748 cm^{-1} (s); $^1\text{H NMR}$ (300 MHz, CDCl_3): δ = 7.55–7.48 (m, 1H; aromatic), 7.26–7.16 (m, 1H; aromatic), 7.04–6.94 (m, 2H; aromatic), 6.88 (distorted d, J = 8.1 Hz, 1H; aromatic), 6.83–6.66 (m, 3H; aromatic), 3.76 (brs, 2H; NH_2), 3.29 ppm (s, 1H; $\equiv\text{CH}$); $^{13}\text{C NMR}$ (75 MHz, CDCl_3): δ = 158.6, 142.7, 138.6, 134.1, 130.2, 125.3, 122.5, 120.5, 118.7, 116.6, 116.0, 112.8, 81.9, 79.4 ppm; GC-MS: m/z (%): 209 (100) [M^+], 183 (32), 180 (77), 168 (57), 152 (19), 139 (5), 108 (9), 89 (9), 80 (39), 65 (16); elemental analysis calcd (%) for $\text{C}_{14}\text{H}_{11}\text{NO}$ (209.24): C 80.36, H 5.30, N 6.69; found: C 80.40, H 5.29, N 6.67.

Compound 1f: Yellow oil; IR (film): $\tilde{\nu}$ = 3466 (w, br), 3377 (w, br), 3280 (m, br), 2107 (vw), 1621 (m), 1510 (m), 1481 (s), 1444 (m), 1305 (w), 1232 (s), 1200 (m), 862 (w), 754 cm^{-1} (m); $^1\text{H NMR}$ (300 MHz, CDCl_3): δ = 7.51 (dd, J = 7.7, 1.8 Hz, 1H; aromatic), 7.24–7.17 (m, 1H; aromatic), 6.97 (td, J = 7.6, 1.1 Hz, 1H; aromatic), 6.80 (distorted d, J = 8.1 Hz, 1H; aromatic), 6.74 (dd, J = 8.4, 0.8 Hz, 1H; aromatic), 6.64–6.59 (m, 1H; aromatic), 6.55–6.50 (m, 1H; aromatic), 3.72 (brs, 2H; NH_2), 3.18 (s, 1H; $\equiv\text{CH}$), 2.38 ppm (s, 3H; Me); $^{13}\text{C NMR}$ (75 MHz, CDCl_3): δ = 159.3, 141.1, 138.6, 135.1, 134.3, 130.2, 122.4, 120.5, 119.4, 117.4, 116.2, 113.2, 81.7, 79.7, 20.9 ppm; GC-MS: m/z (%): 223 (100) [M^+], 208 (11), 194 (24), 183 (34), 182 (23), 168 (17), 152 (8), 122 (11), 94 (20), 77 (18); elemental analysis calcd (%) for $\text{C}_{15}\text{H}_{13}\text{NO}$ (223.27): C 80.69, H 5.87, N 6.27; found: C 80.71, H 5.86, N 6.26.

Compound 1g: Yellow solid; m.p. 36–38 °C; IR (KBr): $\tilde{\nu}$ = 3468 (w, br), 3377 (w, br), 3278 (m, br), 2104 (vw), 1623 (m), 1509 (s), 1481 (m), 1443 (w), 1231 (s), 1208 (s), 1029 (w), 754 cm^{-1} (w); $^1\text{H NMR}$ (300 MHz, CDCl_3): δ = 7.49 (dd, J = 7.6, 1.7 Hz, 1H; aromatic), 7.23–7.15 (m, 1H; aromatic), 6.95 (td, J = 7.5, 1.1 Hz, 1H; aromatic), 6.85 (distorted d, J = 8.5 Hz, 1H; aromatic), 6.72 (dd, J = 8.5, 1.1 Hz, 1H; aromatic), 6.35 (distorted d, J = 2.9 Hz, 1H; aromatic), 6.26 (dd, J = 8.8, 2.9 Hz, 1H; aromatic), 3.74 (s, 5H; OMe + NH_2), 3.31 ppm (s, 1H; $\equiv\text{CH}$); $^{13}\text{C NMR}$ (75 MHz, CDCl_3): δ = 159.7, 157.9, 140.0, 137.2, 134.3, 130.2, 122.2, 121.8, 115.7, 113.0, 104.0, 102.7, 81.8, 79.8, 55.7 ppm; GC-MS: m/z (%): 239 [M^+] (100), 224 (61), 196 (41), 183 (32), 167 (16), 152 (6), 138 (44), 110 (20), 95 (14); elemental analysis calcd (%) for $\text{C}_{15}\text{H}_{13}\text{NO}_2$ (239.27): C 75.30, H 5.48, N 5.85; found: C 75.35, H 5.47, N 5.84.

Compound 1h: Pale yellow solid; m.p. 92–93 °C; IR (KBr): $\tilde{\nu}$ = 3466 (w, br), 3365 (m, br), 3281 (m, br), 2104 (vw), 1674 (m), 1619 (m), 1589 (m), 1507 (w), 1482 (m), 1442 (m), 1359 (w), 1302 (m), 1226 (s), 1195 (m), 755 cm^{-1} (w); $^1\text{H NMR}$ (300 MHz, CDCl_3): δ = 7.56 (d, J = 7.7 Hz, 1H; aromatic), 7.47–7.40 (m, 1H; aromatic), 7.36–7.23 (m, 2H; aromatic), 7.12 (t, J = 7.6 Hz, 1H; aromatic), 6.92 (d, J = 8.2 Hz, 1H; aromatic), 6.74 (d, J = 8.4 Hz, 1H; aromatic), 4.04 (brs, 2H; NH_2), 3.22 (s, 1H; $\equiv\text{CH}$), 2.53 ppm (s, 3H; Me); $^{13}\text{C NMR}$ (75 MHz, CDCl_3): δ = 196.8, 157.5, 148.2, 138.3, 134.6, 134.2, 130.4, 124.0, 119.6, 118.9, 117.6, 115.9, 115.0, 82.3, 79.0, 26.2 ppm; GC-MS: m/z (%): 251 (100) [M^+], 236 (44), 208 (40), 195 (12), 181 (27), 180 (27), 168 (9), 152 (24), 118 (4), 77 (7); elemental analysis calcd (%) for $\text{C}_{16}\text{H}_{13}\text{NO}_2$ (251.28): C 76.48, H 5.21, N 5.57; found: C 76.53, H 5.20, N 5.55.

Compound 1i: Yellow solid; m.p. 63–64 °C; IR (KBr): $\tilde{\nu}$ = 3435 (w, br), 3349 (w, br), 3281 (w, br), 3071 (w), 2106 (vw), 1725 (s), 1621 (m), 1592 (m), 1572 (m), 1509 (m), 1486 (m), 1445 (s), 1302 (s), 1260 (s), 1117 (m), 995 (w), 915 (w), 752 cm^{-1} (m); $^1\text{H NMR}$ (300 MHz, CDCl_3): δ = 7.55 (distorted dd, J = 7.6, 1.4 Hz, 1H; aromatic), 7.52–7.47 (m, 1H; aromatic), 7.41–7.34 (m, 1H; aromatic), 7.34–7.25 (m, 1H; aromatic), 7.10 (td, J = 7.6, 1.0 Hz, 1H; aromatic), 6.90 (dd, J =

8.3, 0.6 Hz, 1H; aromatic), 6.75 (d, $J=8.3$ Hz, 1H; aromatic), 3.87 (s, 5H; OMe + NH₂), 3.24 ppm (s, 1H; $\equiv\text{CH}$); ¹³C NMR (75 MHz, CDCl₃): $\delta=166.9, 157.2, 147.5, 137.9, 134.4, 130.4, 126.1, 123.8, 120.3, 118.3, 117.7, 117.2, 114.3, 82.3, 78.8, 52.0$ ppm; GC-MS: m/z (%): 267 (100) [M^+], 241 (9), 236 (28), 235 (19), 226 (13), 208 (36), 195 (21), 183 (21), 180 (24), 168 (13), 152 (17), 138 (4), 118 (6), 104 (7), 90 (11), 75 (8); elemental analysis calcd (%) for C₁₆H₁₃NO₃ (267.28): C 71.90, H 4.90, N 5.24; found: C 71.94, H 4.89, N 5.23.

Compound 1j: Pale yellow solid; m.p. 104–105 °C; IR (KBr): $\tilde{\nu}=3468$ (w, br), 3360 (w, br), 3283 (w, br), 2225 (m), 1619 (m), 1507 (s), 1402 (m), 1305 (w), 1235 (s), 863 (m), 756 cm⁻¹ (w); ¹H NMR (300 MHz, CDCl₃): $\delta=7.56$ (dd, $J=7.7, 1.6$ Hz, 1H; aromatic), 7.38–7.30 (m, 1H; aromatic), 7.15 (td, $J=7.6, 1.1$ Hz, 1H; aromatic), 7.03 (distorted d, $J=1.8$ Hz, 1H; aromatic), 6.98–6.89 (m, 2H; aromatic), 6.67 (distorted d, $J=8.4$ Hz, 1H; aromatic), 4.20 (brs, 2H; NH₂), 3.21 ppm (s, 1H; $\equiv\text{CH}$); ¹³C NMR (75 MHz, CDCl₃): $\delta=156.8, 147.9, 138.9, 134.7, 130.5, 124.6, 122.7, 119.4, 119.0, 118.7, 117.8, 115.3, 107.7, 82.7, 78.7$ ppm; GC-MS: m/z (%): 234 (100) [M^+], 205 (52), 193 (27), 183 (26), 168 (6), 151 (10), 105 (17), 89 (12), 75 (16); elemental analysis calcd (%) for C₁₅H₁₀N₂O (234.25): C 76.91, H 4.30, N 11.96; found: C 76.96, H 4.28, N 11.95.

Compound 1k: Yellow oil; IR (film): $\tilde{\nu}=3478$ (w, br), 3389 (w, br), 3299 (w, br), 2109 (vw), 1625 (m), 1515 (w), 1484 (m), 1446 (m), 1339 (s), 1229 (s), 1196 (m), 1165 (m), 1119 (m), 862 (w), 755 cm⁻¹ (w); ¹H NMR (300 MHz, CDCl₃): $\delta=7.55$ (distorted dd, $J=7.5$ Hz, 1.1, 1H; aromatic), 7.34–7.24 (m, 1H; aromatic), 7.09 (td, $J=7.5, 1.1$ Hz, 1H; aromatic), 7.05–6.98 (m, 1H; aromatic), 6.95–6.84 (m, 2H; aromatic), 6.80 (distorted d, $J=8.2, 1.1$ Hz; aromatic), 4.08 (brs, 2H; NH₂), 3.25 ppm (s, 1H; $\equiv\text{CH}$); ¹³C NMR (75 MHz, CDCl₃): $\delta=157.2, 146.0, 138.4, 134.4, 130.5, 126.6$ (q, $J=32.4$ Hz), 124.2 (q, $J=271.9$ Hz), 123.9, 118.4, 118.0, 115.4 (q, $J=4.2$ Hz), 114.1, 112.8 (q, $J=3.7$ Hz), 82.4, 78.9 ppm; ¹⁹F NMR (471 MHz, CDCl₃): $\delta=-62.6$ ppm (s, 3F; CF₃); GC-MS: m/z (%): 277 (100) [M^+], 248 (25), 236 (28), 208 (14), 180 (21), 148 (11), 128 (3), 101 (7), 75 (9); elemental analysis calcd (%) for C₁₅H₁₀F₃NO (277.24): C 64.98, H 3.64, F 20.56, N 5.05; found: C 65.03, H 3.63, F 20.57, N 5.03.

General procedure for the oxidative carbonylation of 1a–g to give 2a–d [Eq. (1)]

A 35 mL stainless-steel autoclave was charged in the presence of air with PdI₂ (2.5 mg, 6.94 × 10⁻³ mmol), KI (11.5 mg, 6.93 × 10⁻² mmol), and a solution of **1** [0.35 mmol: **1a** (100 mg), **1b** (127 mg), **1c** (101 mg), **1d** (93 mg)] in MeOH (7.0 mL). The autoclave was sealed and, while the mixture was stirred, the autoclave was pressurized with CO (32 atm) and air (up to 40 atm). After being stirred at 100 °C for the required time (24 h for **1a–c**; 48 h for **1d**), the autoclave was cooled, degassed, and opened. The solvent was evaporated and the products were purified by column chromatography on silica gel to give pure **2a–d** (eluent: 7:3 hexane/AcOEt for **2a** and **2b**; 8:2 hexane/AcOEt for **2c** and **2d**): **2a**, yellow oil, 90 mg, 74%; **2b**, yellow solid, 86 mg, 58%; **2c**, yellow oil, 61 mg, 50%; **2d**, yellow oil, 70 mg, 62%.

General procedure for the oxidative carbonylation of 1e–k to give 3e–i and 3e'–k' (Table 1)

A 35 mL stainless-steel autoclave was charged in the presence of air with PdI₂ (2.5 mg, 6.94 × 10⁻³ mmol), KI (11.5 mg, 6.93 × 10⁻² mmol), and a solution of **1** [0.35 mmol; **1e** (73 mg), **1f** (78 mg), **1g** (84 mg), **1h** (88 mg), **1i** (94 mg), **1j** (82 mg), **1k** (97 mg)] in ROH (R=Me or Et; 7 mL). The autoclave was sealed and, while the mixture was stirred, the autoclave was pressurized

with CO (32 atm) and air (up to 40 atm). After being stirred at 100 °C for the required time (15 h for the reaction of **1e–i** with MeOH; 24 h for the reactions of **1e–k** with EtOH), the autoclave was cooled, degassed, and opened. The solvent was evaporated and the product was purified by column chromatography on silica gel to give pure **3e–i** (R=Me) for 6:4 hexane/AcOEt as the eluent or **3e'–3k'** (R=Et) for 65:35 hexane/AcOEt as the eluent: **3e**, yellow solid, 65 mg, 63%; **3e'**, white solid, 77 mg, 71%; **3f**, yellow solid, 78 mg, 72%; **3f'**, yellow solid, 79 mg, 70%; **3g**, yellow solid, 71 mg, 62%; **3g'**, gray solid, 89 mg, 75%; **3h**, white solid, 86 mg, 73%; **3h'**, yellow oil, 85 mg, 69%; **3i**, white solid, 89 mg, 72%; **3i'**, white solid, 81 mg, 63%; **3j'**, 87 mg, 74%; **3k'**, colorless solid, 70 mg, 53%.

Compound 2a: Yield: 90 mg (74% from **1a**); yellow oil; IR (film): $\tilde{\nu}=3427$ (m, br), 2220 (vw), 1739 (s), 1610 (m), 1529 (s), 1454 (s), 1326 (w), 1253 (s), 1065 (m), 753 cm⁻¹ (s); ¹H NMR (300 MHz, CDCl₃): $\delta=8.26$ –8.16 (m, 1H; NH), 7.59 (dd, $J=7.7, 1.4$ Hz, 1H; aromatic), 7.39–7.22 (m, 7H; aromatic), 7.22–7.07 (m, 2H; aromatic), 7.07–6.91 (m, 2H; aromatic), 6.80 (distorted dd, $J=8.1, 1.3$ Hz, 1H; aromatic), 3.73 ppm (s, 3H; CO₂Me); ¹³C NMR (75 MHz, CDCl₃): $\delta=156.5, 153.9, 145.6, 133.8, 131.6, 129.8, 129.4, 128.4, 128.3, 124.3, 123.9, 122.9, 119.5, 119.2, 117.0, 116.1, 94.9, 84.4, 52.3$ ppm; GC-MS: m/z (%): 343 (66) [M^+], 311 (20), 310 (22), 283 (29), 282 (27), 268 (59), 254 (30), 244 (100), 241 (31), 226 (7), 209 (11), 176 (13), 165 (16), 150 (10), 127 (8), 91 (3), 77 (8); elemental analysis calcd (%) for C₂₂H₁₇NO₃ (343.38): C 76.95, H 4.99, N 4.08; found: C 76.98, H 4.98, N 4.06.

Compound 2b: Yield: 86 mg (58% from **1b**); yellow solid; m.p. 58–60 °C; IR (KBr): $\tilde{\nu}=3459$ (w, br), 2175 (vw), 1739 (s), 1608 (w), 1524 (s), 1474 (m), 1452 (m), 1323 (w), 1227 (s), 1208 (s), 1060 (m), 820 (m), 756 cm⁻¹ (m); ¹H NMR (300 MHz, CDCl₃): $\delta=8.20$ (brd, $J=7.6$ Hz, 1H; NH), 7.57 (dd, $J=7.7, 1.4$ Hz, 1H; aromatic), 7.48–7.38 (m, 3H; aromatic), 7.33 (td, $J=8.2, 1.7$ Hz, 1H; aromatic), 7.22–7.15 (m, 3H; aromatic), 7.14–7.07 (m, 1H; aromatic), 7.01 (distorted d, $J=8.2$ Hz, 1H; aromatic), 6.95 (td, $J=8.1, 1.5$ Hz, 1H; aromatic), 6.78 (distorted dd, $J=8.2, 1.2$ Hz, 1H; aromatic), 3.74 ppm (s, 3H; CO₂Me); ¹³C NMR (75 MHz, CDCl₃): $\delta=156.4, 153.9, 145.5, 133.7, 133.0, 131.6, 130.1, 129.3, 124.3, 123.9, 123.0, 122.7, 121.8, 119.6, 119.2, 116.9, 115.6, 93.8, 85.5, 52.3$ ppm; GC-MS: m/z (%) 423 (100) [$M+2^+$], 421 (98) [M^+], 391 (22), 389 (20), 348 (32), 346 (35), 324 (97), 322 (99), 310 (29), 254 (65), 241 (64), 209 (18), 176 (27), 150 (20), 126 (16), 113 (12); elemental analysis calcd (%) for C₂₂H₁₆BrNO₃ (422.27): C 62.57, H 3.82, Br 18.92, N 3.32; found: C 62.61, H 3.83, Br 18.94, N 3.31.

Compound 2c: Yield: 61 mg (50% from **1c**); yellow oil; IR (film): $\tilde{\nu}=3433$ (w, br), 3366 (w, br), 2929 (m), 2858 (w), 2208 (vw), 1740 (s), 1609 (w), 1529 (s), 1479 (m), 1445 (s), 1227 (s), 1065 (w), 751 cm⁻¹ (m); ¹H NMR (300 MHz, CDCl₃): $\delta=8.22$ –8.11 (m, 1H; NH), 7.47 (distorted dd, $J=7.7, 1.7$ Hz, 1H; aromatic), 7.30–7.22 (m, 2H; aromatic), 7.15–7.03 (m, 2H; aromatic), 7.00–6.88 (m, 2H; aromatic), 6.74 (distorted dd, $J=8.2, 1.2$ Hz, 1H; aromatic), 6.09–6.01 (m, 1H; =CH), 3.78 (s, 3H; CO₂Me), 2.16–1.96 (m, 4H; cyclohexenyl ring), 1.67–1.49 ppm (m, 4H; cyclohexenyl ring); ¹³C NMR (75 MHz, CDCl₃): $\delta=156.1, 153.9, 145.7, 135.7, 133.6, 129.3, 129.2, 124.2, 123.6, 122.8, 120.5, 119.6, 119.0, 117.3, 116.8, 96.9, 81.7, 52.3, 28.8, 25.8, 22.3, 21.5$ ppm; GC-MS: m/z (%): 347 (100) [M^+], 319 (64), 315 (23), 304 (62), 286 (54), 278 (26), 272 (89), 260 (45), 245 (36), 231 (24), 218 (10), 208 (50), 194 (17), 183 (27), 165 (36), 152 (23), 139 (12), 115 (15); elemental analysis calcd (%) for C₂₂H₂₁NO₃ (347.41): C 76.06, H 6.09, N 4.03; found: C 76.12, H 6.08, N 4.04.

Compound 2d: Yield: 70 mg (62% from **1d**); yellow oil; IR (film): $\tilde{\nu}=3435$ (m, br), 2969 (m), 2931 (m), 2867 (w), 2242 (w), 1739 (s), 1611 (m), 1539 (m), 1480 (w), 1456 (m), 1328 (w), 1219 (m), 1113

(w), 1065 (m), 954 (w), 755 cm^{-1} (s); ^1H NMR (300 MHz, CDCl_3): δ = 8.16 (brd, J = 9.1 Hz, 1H; NH), 7.45 (distorted dd, J = 7.7, 1.4 Hz, 2H; aromatic), 7.31–7.23 (m, 1H; aromatic), 7.16–6.98 (m, 3H; aromatic), 6.91 (td, J = 8.1, 1.5 Hz, 1H; aromatic), 6.65 (distorted dd, J = 8.1, 1.2 Hz, 1H; aromatic), 3.79 (s, 3H; CO_2Me), 1.12 ppm (s, 9H; tBu); ^{13}C NMR (75 MHz, CDCl_3): δ = 155.8, 154.0, 146.1, 133.8, 128.9, 124.5, 123.2, 122.7, 120.3, 119.0, 115.9, 104.7, 89.1, 73.9, 52.3, 30.6, 28.0 ppm; GC-MS: m/z (%): 323 (97) [M^+], 308 (33), 291 (9), 276 (100), 266 (31), 248 (46), 234 (43), 233 (33), 219 (14), 209 (13), 178 (5), 165 (4), 152 (5), 141 (10), 128 (8), 115 (10); elemental analysis calcd (%) for $\text{C}_{20}\text{H}_{21}\text{NO}_3$ (323.39): C 74.28, H 6.55, N 4.33; found: C 74.33, H 6.53, N 4.32.

Compound 3e: Yield: 65 mg (63% from **1e**; Table 1, entry 1); yellow solid; m.p. 223–225 °C; IR (KBr): $\tilde{\nu}$ = 3468 (w, br), 3378 (m, br), 2952 (w), 1723 (s), 1622 (m), 1503 (m), 1483 (m), 1435 (m), 1354 (w), 1306 (w), 1268 (m), 1216 (s), 755 cm^{-1} (m); ^1H NMR (300 MHz, CDCl_3): δ = 7.89 (brs, 1H; NH), 7.47–7.05 (m, 8H; aromatic), 5.79 (s, 1H; =CH), 3.74 ppm (s, 3H; CO_2Me); ^{13}C NMR (75 MHz, CDCl_3): δ = 168.9, 164.3, 157.0, 152.4, 149.9, 131.9, 131.7, 130.5, 129.2, 126.7, 126.4, 126.3, 125.1, 123.2, 121.3, 120.0, 51.6 ppm; GC-MS: m/z (%): 295 (59) [M^+], 278 (12), 263 (97), 236 (97), 235 (100), 207 (29), 190 (14), 180 (36), 165 (28), 152 (35), 139 (6), 104 (10), 89 (17), 75 (13); elemental analysis calcd (%) for $\text{C}_{17}\text{H}_{13}\text{NO}_4$ (295.29): C 69.15, H 4.44, N 4.74; found: C 69.19, H 4.43, N 4.73.

Compound 3e': Yield: 77 mg (71% from **1e**; Table 1, entry 2); white solid; m.p. 231–233 °C. IR (KBr): $\tilde{\nu}$ = 3291 (w, br), 2926 (w), 1716 (s), 1674 (m), 1500 (w), 1470 (m), 1446 (m), 1384 (m), 1290 (w), 1260 (w), 1217 (m), 1190 (m), 1107 (w), 1032 (w), 755 cm^{-1} (s); ^1H NMR (300 MHz, CDCl_3): δ = 7.89 (brs, 1H; NH), 7.47–7.09 (m, 8H; aromatic), 5.79 (s, 1H; =CH), 4.20 (q, J = 7.1 Hz, 2H; CH_2CH_3), 1.29 ppm (t, J = 7.1 Hz, 3H; CH_2CH_3); ^{13}C NMR (75 MHz, CDCl_3): δ = 169.2, 163.8, 156.6, 151.9, 149.3, 131.9, 131.7, 130.4, 129.2, 126.7, 126.3, 126.0, 125.0, 123.1, 121.2, 120.3, 60.8, 14.1 ppm; GC-MS: m/z (%): 309 (37) [M^+], 281 (6), 264 (33), 263 (73), 236 (100), 235 (75), 219 (6), 207 (21), 190 (8), 180 (26), 165 (18), 152 (21), 89 (7); elemental analysis calcd (%) for $\text{C}_{18}\text{H}_{13}\text{NO}_4$ (309.32): C 69.89, H 4.89, N 4.53; found: C 69.93, H 4.88, N 4.54.

Compound 3f: Yield: 78 mg (72% from **1f**; Table 1, entry 3); pale yellow solid; m.p. 205–207 °C; IR (KBr): $\tilde{\nu}$ = 3307 (br), 1721 (s), 1673 (s), 1478 (w), 1448 (w), 1385 (m), 1211 (m), 1173 (m), 757 cm^{-1} (s); ^1H NMR (300 MHz, CDCl_3): δ = 7.87 (brs, 1H; NH), 7.47–7.28 (m, 3H; aromatic), 7.21–6.93 (m, 4H; aromatic), 5.80 (s, 1H; =CH), 3.75 (s, 3H; CO_2Me), 2.30 ppm (s, 3H; Me at C-3); ^{13}C NMR (75 MHz, CDCl_3): δ = 169.0, 164.4, 157.1, 150.2, 150.0, 136.5, 131.8, 131.7, 130.5, 129.8, 127.1, 126.5, 125.0, 122.8, 121.3, 119.9, 51.6, 20.8 ppm; GC-MS: m/z (%): 309 (94) [M^+], 277 (100), 250 (99), 249 (95), 235 (15), 221 (39), 207 (93), 193 (54), 179 (31), 165 (15), 147 (21), 135 (28), 89 (25), 73 (46); elemental analysis calcd (%) for $\text{C}_{18}\text{H}_{13}\text{NO}_4$ (309.32): C 69.89, H 4.89, N 4.53; found: C 69.92, H 4.90, N 4.52.

Compound 3f': Yield: 79 mg (70% from **1f**; Table 1, entry 4); yellow solid; m.p. 220–222 °C; IR (KBr): $\tilde{\nu}$ = 3396 (m, br), 1712 (s), 1674 (s), 1501 (w), 1477 (w), 1385 (m), 1305 (w), 1275 (w), 1209 (m), 1180 (m), 1037 (w), 758 cm^{-1} (m); ^1H NMR (300 MHz, CDCl_3): δ = 8.32 (brs, 1H; NH), 7.47–7.29 (m, 3H; aromatic), 7.20–6.95 (m, 4H; aromatic), 5.80 (s, 1H; =CH), 4.22 (q, J = 7.1 Hz, 2H; CH_2CH_3), 2.29 (s, 3H; Me at C-3), 1.30 ppm (t, J = 7.1 Hz, 3H; CH_2CH_3); ^{13}C NMR (75 MHz, CDCl_3): δ = 169.0, 163.9, 157.1, 150.2, 149.7, 136.4, 131.9, 131.6, 130.5, 129.7, 127.2, 126.5, 124.9, 122.8, 121.3, 120.4, 60.8, 20.8, 14.2 ppm; GC-MS: m/z (%): 323 (39) [M^+], 295 (5), 278 (33), 277 (66), 250 (100), 249 (79), 232 (7), 221 (17), 207 (14), 193 (18), 179 (15), 165 (11), 152 (9), 139 (3), 128 (4), 101 (6), 89 (9), 77 (8); elemental analysis calcd (%) for $\text{C}_{19}\text{H}_{17}\text{NO}_4$ (323.34): C 70.58, H 5.30, N 4.33; found: C 70.61, H 5.29, N 4.31.

Compound 3g: Yield: 71 mg (62% from **1g**; Table 1, entry 5); yellow solid; m.p. 243–245 °C; IR (KBr): $\tilde{\nu}$ = 3429 (m, br), 2922 (w), 1709 (s), 1677 (s), 1607 (m), 1495 (w), 1476 (w), 1373 (w), 1258 (w), 1200 (s), 1161 (m), 1030 (m), 756 cm^{-1} (m); ^1H NMR (300 MHz, CDCl_3): δ = 7.47–7.28 (m, 4H; NH + 3H aromatic), 7.20–7.11 (m, 1H; aromatic), 7.05–6.98 (m, 1H; aromatic), 6.81–6.72 (m, 2H; aromatic), 5.81 (s, 1H; =CH), 3.76 (s, 3H; CO_2Me), 3.74 ppm (s, 3H; OMe at C-3); ^{13}C NMR (75 MHz, CDCl_3): δ = 168.7, 164.4, 157.8, 157.3, 150.1, 146.4, 132.7, 131.7, 130.5, 127.0, 124.9, 123.7, 121.2, 119.8, 115.2, 111.1, 56.0, 51.6 ppm; GCMS: m/z (%): 325 (68) [M^+], 308 (4), 297 (11), 294 (41), 278 (20), 266 (100), 265 (71), 250 (41), 238 (20), 222 (31), 210 (10), 195 (16), 180 (6), 167 (23), 139 (13), 115 (4), 101 (9), 89 (7); elemental analysis calcd (%) for $\text{C}_{18}\text{H}_{15}\text{NO}_5$ (325.32): C 66.46, H 4.65, N 4.31; found: C 66.49, H 4.64, N 4.30.

Compound 3g': Yield: 89 mg (75% from **1g**; Table 1, entry 6); off-white solid; m.p. 219–221 °C; IR (KBr): $\tilde{\nu}$ = 3294 (m, br), 2927 (w), 1712 (s), 1676 (s), 1609 (m), 1502 (m), 1477 (m), 1390 (m), 1270 (m), 1208 (s), 1180 (s), 1032 (m), 760 cm^{-1} (m); ^1H NMR (300 MHz, CDCl_3): δ = 7.91 (brs, 1H; NH), 7.46–7.28 (m, 3H; aromatic), 7.20–7.11 (m, 1H; aromatic), 7.0 (distorted d, J = 8.8 Hz, 1H; aromatic), 6.83–6.72 (m, 2H; aromatic), 5.80 (s, 1H; =CH), 4.21 (q, J = 7.1 Hz, 2H; CH_2CH_3), 3.76 (s, 3H; OMe), 1.29 ppm (t, J = 7.1 Hz, 3H; CH_2CH_3); ^{13}C NMR (75 MHz, CDCl_3): δ = 168.8, 164.0, 157.8, 157.3, 149.7, 146.3, 132.8, 131.5, 130.5, 127.1, 124.9, 123.6, 121.1, 120.3, 115.1, 111.1, 60.8, 56.0, 14.2 ppm; GC-MS: m/z (%): 339 (52) [M^+], 311 (8), 294 (31), 293 (41), 278 (17), 266 (100), 265 (68), 250 (37), 238 (22), 222 (23), 207 (13), 195 (15), 178 (7), 167 (23), 152 (8), 139 (11), 115 (4), 101 (9), 89 (7); elemental analysis calcd (%) for $\text{C}_{19}\text{H}_{17}\text{NO}_5$ (339.34): C 67.25, H 5.05, N 4.13; found: C 67.30, H 5.03, N 4.12.

Compound 3h: Yield: 86 mg (73% from **1h**; Table 1, entry 7); colorless solid; m.p. 265–267 °C; IR (KBr): $\tilde{\nu}$ = 3425 (w, br), 2952 (w), 1721 (s), 1673 (s), 1598 (w), 1448 (w), 1389 (w), 1283 (m), 1199 (s), 854 (w), 768 cm^{-1} (w); ^1H NMR (300 MHz, $[\text{D}_6]\text{DMSO}$): δ = 10.4 (brs, 1H; NH), 7.93–7.83 (m, 1H; aromatic), 7.65 (brs, 1H; aromatic), 7.61–7.21 (m, 5H; aromatic), 5.89 (s, 1H; =CH), 3.65 (s, 3H; CO_2Me), 2.55 ppm (s, 3H; MeCO); ^{13}C NMR (75 MHz, $[\text{D}_6]\text{DMSO}$): δ = 196.4, 167.6, 163.6, 155.3, 154.0, 149.3, 134.7, 133.2, 132.0, 130.3, 128.9, 126.4, 125.4, 124.5, 123.2, 121.1, 119.2, 51.5, 26.6 ppm; GC-MS: m/z (%): 337 (47) [M^+], 305 (48), 279 (100), 278 (65), 262 (41), 261 (31), 249 (12), 235 (22), 222 (15), 206 (21), 191 (7), 178 (14), 166 (10), 151 (18), 139 (15), 89 (10); elemental analysis calcd (%) for $\text{C}_{19}\text{H}_{15}\text{NO}_5$ (337.33): C 67.65, H 4.48, N 4.15; found: C 67.69, H 4.46, N 4.15.

Compound 3h': Yield: 85 mg (69% from **1h**; Table 1, entry 8); colorless solid; m.p. 271–273; IR (KBr): $\tilde{\nu}$ = 3342 (w, br), 2982 (w), 1723 (s), 1683 (m), 1596 (w), 1432 (w), 1263 (m), 1207 (s), 1027 (w), 759 cm^{-1} (w); ^1H NMR (300 MHz, $[\text{D}_6]\text{DMSO}$): δ = 10.4 (brs, 1H; NH), 7.89 (distorted dd, J = 8.5, 2.1 Hz, 1H; aromatic), 7.83 (d, J = 2.1 Hz, 1H; aromatic), 7.60–7.23 (m, 5H; aromatic), 5.85 (s, 1H; =CH), 4.12 (q, J = 7.0 Hz, 2H; CH_2CH_3), 2.55 (s, 3H; MeCO), 1.21 ppm (t, J = 7.0 Hz, 3H; CH_2CH_3); ^{13}C NMR (75 MHz, $[\text{D}_6]\text{DMSO}$): δ = 196.3, 167.6, 163.2, 155.3, 154.0, 148.9, 134.7, 133.3, 131.9, 130.3, 129.0, 126.4, 125.4, 124.5, 123.2, 121.0, 119.6, 60.2, 26.6, 13.9 ppm; GC-MS: m/z (%): 351 (39) [M^+], 323 (3), 306 (7), 278 (45), 262 (25), 236 (100), 207 (11), 192 (6), 180 (8), 165 (30), 152 (11); elemental analysis calcd (%) for $\text{C}_{20}\text{H}_{17}\text{NO}_5$ (351.35): C 68.37, H 4.88, N 3.99; found: C 68.40, H 4.88, N 4.00.

Compound 3i: Yield: 89 mg (72% from **1i**; Table 1, entry 9); colorless solid; m.p. 244–246 °C; IR (KBr): $\tilde{\nu}$ = 3512 (m, br), 1721 (s), 1675 (m), 1398 (m), 1280 (w), 1201 cm^{-1} (w); ^1H NMR (300 MHz, CDCl_3): δ = 8.02–7.82 (m, 4H; NH + 3H aromatic), 7.52–7.30 (m, 2H; aromatic), 7.25–7.15 (m, 2H; aromatic), 5.83 (s, 1H; =CH), 3.91 (s, 3H;

CO₂Me), 3.77 ppm (s, 3H; CO₂Me); ¹³C NMR (75 MHz, CDCl₃): δ = 169.0, 165.6, 164.1, 156.0, 155.1, 149.0, 132.1, 132.0, 130.5, 130.4, 128.4, 127.3, 126.6, 125.5, 123.3, 121.3, 120.4, 52.4, 52.0 ppm; GC-MS: *m/z* (%): 353 (80) [*M*⁺], 322 (40), 321 (74), 294 (100), 293 (58), 262 (41), 235 (20), 206 (26), 178 (19), 151 (11), 131 (11), 89 (11); elemental analysis calcd (%) for C₁₉H₁₅NO₆ (353.33): C 64.59, H 4.28, N 3.96; found: C 64.63, H 4.27, N 3.97.

Compound 3i: Yield: 81 mg (63% from **1i**; Table 1, entry 10); white solid; m.p. 220–222 °C; IR (KBr): $\tilde{\nu}$ = 3461 (m, br), 1720 (s), 1682 (m), 1400 (m), 1283 (m), 1178 (m), 1100 (w), 759 cm⁻¹ (w); ¹H NMR (300 MHz, [D₆]DMSO): δ = 10.43 (brs, 1H; NH), 7.85 (dist dd, *J* = 8.5, 2.2 Hz, 1H; aromatic), 7.70 (d, *J* = 2.2 Hz, 1H; aromatic), 7.61–7.23 (m, 5H; aromatic), 5.86 (s, 1H; =CH), 4.12 (q, *J* = 7.1 Hz, 2H; CH₂CH₃), 3.84 (s, 3H; CO₂Me), 1.21 ppm (t, *J* = 7.1 Hz, 3H; CH₂CH₃); ¹³C NMR (75 MHz, DMSO): δ = 167.6, 164.9, 163.2, 155.2, 154.0, 148.9, 133.3, 131.9, 130.3, 129.3, 127.5, 126.3, 125.9, 125.5, 123.5, 121.0, 119.7, 60.3, 52.3, 13.8 ppm; GC-MS: *m/z* (%): 367 (55) [*M*⁺], 339 (7), 322 (35), 321 (61), 294 (100), 293 (49), 262 (28), 235 (15), 108 (17), 178 (15), 152 (8), 131 (4), 89 (7); elemental analysis calcd (%) for C₂₀H₁₇NO₆ (367.35): C 65.39, H 4.66, N 3.81; found: C 65.42, H 4.64, N 3.83.

Compound 3j: Yield: 87 mg (74% from **1j**; Table 1, entry 11); colorless solid; m.p. 249–251 °C; IR (KBr): $\tilde{\nu}$ = 3396 (m, br), 2233 (vw), 1712 (s), 1670 (m), 1634 (w), 1477 (w), 1385 (m), 1198 (m), 1026 (m), 767 cm⁻¹ (w); ¹H NMR (300 MHz, [D₆]DMSO): δ = 10.45 (brs, 1H; NH), 7.78 (distorted dd, *J* = 8.4, 2.1 Hz, 1H; aromatic), 7.63–7.40 (m, 5H; aromatic), 7.33–7.25 (m, 1H; aromatic), 5.89 (s, 1H; =CH), 4.15 (q, *J* = 7.1 Hz, 2H; CH₂CH₃), 1.23 ppm (t, *J* = 7.1 Hz, 3H; CH₂CH₃); ¹³C NMR (75 MHz, [D₆]DMSO): δ = 167.5, 163.2, 155.2, 154.1, 148.3, 134.6, 132.5, 131.9, 130.1, 129.1, 126.6, 125.6, 124.6, 121.1, 120.4, 117.4, 109.2, 60.4, 13.9 ppm; GC-MS: *m/z* (%): 334 (16) [*M*⁺], 288 (68), 261 (100), 260 (63), 247 (10), 232 (22), 216 (11), 205 (29), 190 (22), 177 (19), 164 (5), 151 (20), 116 (6), 101 (18), 89 (24), 75 (27); elemental analysis calcd (%) for C₁₉H₁₄N₂O₄ (334.33): C 68.26, H 4.22, N 8.38; found: C 68.31, H 4.21, N 8.39.

Compound 3k: Yield: 70 mg (53% from **1k**; Table 1, entry 12); colorless solid; m.p. 218–220 °C; IR (KBr): $\tilde{\nu}$ = 3103 (m, br), 1718 (s), 1673 (m), 1504 (m), 1478 (m), 1449 (m), 1391 (m), 1339 (s), 1198 (m), 1167 (m), 1126 (m), 882 (w), 856 (w), 767 cm⁻¹ (w); ¹H NMR (300 MHz, [D₆]DMSO): δ = 10.48 (brs, 1H; NH), 7.71–7.63 (m, 1H; aromatic), 7.61–7.39 (m, 5H; aromatic), 7.33–7.24 (m, 1H; aromatic), 5.89 (s, 1H; =CH), 4.13 (q, *J* = 7.1 Hz, 2H; CH₂CH₃), 1.20 ppm (t, *J* = 7.1 Hz, 3H; CH₂CH₃); ¹³C NMR (75 MHz, [D₆]DMSO): δ = 167.6, 163.2, 155.1, 153.2, 148.7, 134.0, 132.0, 130.3, 126.8 (q, *J* = 32.6 Hz), 126.3, 125.6, 125.5 (q, *J* = 1.5 Hz), 124.3, 123.4 (q, *J* = 272.2 Hz), 121.1, 120.0, 60.3, 13.8 ppm; ¹⁹F NMR (471 MHz, CDCl₃): δ = -60.6 ppm (s, 3F; CF₃); GC-MS: *m/z* (%): 377 (45) [*M*⁺], 349 (5), 332 (28), 331 (58), 305 (17), 304 (100), 276 (20), 275 (22), 248 (19), 234 (5), 208 (8), 207 (12), 178 (13), 152 (9), 128 (5), 101 (11), 89 (12), 75 (18); elemental analysis calcd (%) for C₁₉H₁₄F₃NO₄ (377.31): C 60.48, H 3.74, F 15.11, N 3.71; found: C 68.45, H 3.72, F 15.13, N 3.73.

Theoretical calculations

Quantum calculations were carried out by using the NWChem package,^[13] within the framework of DFT. Becke–Lee–Yang–Parr16 (B3LYP) hybrid potentials and energy functionals were used to take into account the exchange and correlation contributions. The Coulomb and exchange-correlation potentials were numerically integrated on an adaptive grid with fine accuracy. All calculations were performed by using linear combinations of Gaussian-type orbitals: triple- ζ basis set with polarization function (6-311G*) for C, N, O, and H atoms and 3-21G* basis set for iodine. Relativistic effective

core potential (LANL2DZ ECP)^[13] was used instead for the palladium atom. The convergence threshold was set to 10⁻⁶ a.u. for the self-consistent field procedure and to 10⁻⁵ a.u. for the electron density root-mean-square. All structures were fully optimized by using analytical gradients with approximate Hessian updates. The optimization convergences, based on the maximum and root-mean-square gradient thresholds, were set equal to 10⁻⁶ a.u., whereas the maximum and root-mean-square of the Cartesian displacement vectors were set to 6 × 10⁻⁶ and 4 × 10⁻⁶ a.u., respectively. An accurate characterization of the structures on the PES required very high convergence criteria for Hessian evaluation. Thus, in the Hessian calculations, the energy convergence threshold was set to 10⁻⁸ a.u. for the self-consistent field procedure and 10⁻⁷ a.u. for the electron density root-mean-square.

Cell cultures

Human breast cancer epithelial cell line MCF-7 (ER-positive) was cultured in Dulbecco's modified Eagle's medium (DMEM) containing 5% fetal bovine serum (FBS), 1% L-glutamine, 1% Eagle's non-essential amino acids, and 1 mg mL⁻¹ penicillin–streptomycin at 37 °C with 5% CO₂ in air. Triple-negative human breast cancer cell line MDA-MB-231 (ER-, PR-, HER2-negative) was cultured in DMEM:F12 containing 5% FBS. Human normal breast epithelial cell line MCF-10A was grown in DMEM-F12 medium containing 5% horse serum. Before each experiment, cells were grown in phenol red free medium, containing 5% charcoal-stripped FBS for 2 days and treated as described.

Cell viability assays

Cell viability was determined with the MTT (Sigma, Milan, Italy) assay. MCF-7, MDA-MB-231, and MCF-10A cells (2 × 10⁴ cells mL⁻¹) were grown in 24-well plates and exposed to treatments as indicated for 96 h, in phenol red free minimum essential medium (MEM) containing 5% charcoal-stripped FBS. The MTT assay was performed as follows: 100 μL MTT stock solution in PBS (2 mg mL⁻¹) was added to each well and incubated at 37 °C for 2 h, followed by media removal, and solubilization in DMSO (500 μL). After shaking the plates for 15 min, the absorbance in each well, including the blanks at λ = 570 nm, was measured by using a Beckman Coulter spectrophotometer. Data are representative of three independent experiments, each performed in triplicate. Data were analyzed for statistical significance by using a two-tailed Student's *t*-test, performed by using the Graph Pad Prism 4 program (Graph Pad Software, Inc., San Diego, CA). SD values are shown. A minimum of three experiments, containing eight different doses of ζ -lactam **3j** in triplicate, was combined for IC₅₀ calculations. The absorbance readings were used to determine the IC₅₀ values by using the GraphPad Prism 4 program. Briefly, values were log-transformed, then normalized, and nonlinear regression analysis was used to generate a sigmoidal dose-response curve to calculate IC₅₀ values for each cell line.

Soft-agar anchorage-independent growth assays

Cells (10⁴ per well) were plated in 0.35% agarose (4 mL) with 5% charcoal-stripped FBS in phenol red free media, with a 0.7% agarose base in 6-well plates. Two days after plating, media containing vehicle or ζ -lactam **3j** were added to the top layer and replaced every two days. After 14 days, MTT (300 μL) was added to each well and allowed to incubate at 37 °C for 4 h. Plates were then placed at 4 °C overnight and colonies of > 50 μm in diameter from triplicate assays were counted. Data are the mean colony number

of three plates and representative of two independent experiments, analyzed for statistical significance by using a two-tailed Student's t-test, performed by using the Graph Pad Prism 4 program (GraphPad Software, Inc., San Diego, CA).

Wound-healing scratch assays

Motility was assessed by wound-healing scratch assays. Briefly, cell monolayers were scraped and treated as indicated. Wound closure was monitored over 24 h; cells were fixed and stained with Coomassie brilliant blue. Pictures were taken at 10× magnification by means of phase-contrast microscopy and were representative of three independent experiments.

Keywords: antitumor agents · carbonylation · heterocycles · palladium · reaction mechanisms

- [1] For recent representative examples, see: a) R. A. Bauer, T. A. Wenderski, D. S. Tan, *Nat. Chem. Biol.* **2012**, *9*, 21–29; b) J. Mallinson, I. Collins, *Future Med. Chem.* **2012**, *4*, 1409–1438; c) T. Kitayama, A. Saito, S. Ohta, *Tetrahedron: Asymmetry* **2012**, *23*, 1490–1495; d) S. Zheng, L. Lariaia, C. J. O'Connor, D. Sorrel, Y. S. Tan, Z. Xu, A. R. Venkitaraman, W. Wu, D. R. Spring, *Org. Biomol. Chem.* **2012**, *10*, 2590–2593.
- [2] For examples, see: a) J. Alberta Marco, M. Carda, *Nat. Prod. Commun.* **2011**, *6*, 505–514; b) X. Su, G. L. Thomas, W. R. J. D. Galloway, D. S. Surry, R. J. Spandl, D. R. Spring, *Synthesis* **2009**, 3880–3896; c) J. K. Mishra, G. Panda, *J. Comb. Chem.* **2007**, *9*, 321–338; d) P. Arya, S. Couve-Bonnaire, P. Durieux, D. Laforce, R. Kumar, D. M. Leek, *J. Comb. Chem.* **2004**, *6*, 735–745.
- [3] For recent reviews on the preparation of medium-sized rings, see: a) A. Hussain, S. K. Yousuf, D. Mukherjee, *RSC Adv.* **2014**, *4*, 43241–43257; b) P. Trapencieris, J. Strazdina, P. Bertrand, *Chem. Heterocycl. Compd.* **2012**, *48*, 833–855; c) K. C. Majumdar, *RSC Adv.* **2011**, *1*, 1152–1170.
- [4] a) G. Illuminati, L. Mandolini, *Acc. Chem. Res.* **1981**, *14*, 95–102; b) E. L. Eliel, S. H. Wilen, *Stereochemistry of Organic Compounds*, Wiley, Chichester, **1994**.
- [5] For recent reviews, see: a) W. Fang, H. Zhu, Q. Deng, S. Liu, X. Liu, Y. Shen, T. Tu, *Synthesis* **2014**, *46*, 1689–1708; b) X.-F. Wu, H. Neumann, M. Beller, *Chem. Rev.* **2013**, *113*, 1–35; c) X.-F. Wu, H. Neumann, M. Beller, *ChemSusChem* **2013**, *6*, 229–241; d) B. Gabriele, R. Mancuso, G. Salerno, *Eur. J. Org. Chem.* **2012**, 6825–6839; e) X.-F. Wu, H. Neumann, *ChemCatChem* **2012**, *4*, 447–458.
- [6] For some representative recent examples, see: a) H. Yu, G. Zhang, H. Huang, *Angew. Chem. Int. Ed.* **2015**, *54*, 10912–10916; *Angew. Chem.* **2015**, *127*, 11062–11066; b) F. Ji, X. Li, W. Guo, W. Wu, H. Jiang, *J. Org. Chem.* **2015**, *80*, 5713–5718; c) J. El Karroumi, A. Al Haib, E. Manoury, A. Benharref, J. C. Daran, M. Gouygou, M. Urrutigoity, *J. Mol. Catal. A* **2015**, *401*, 18–26; d) Y. Xu, J. Zhao, H. Chen, W. Wu, H. Jiang, *Chem. Commun.* **2014**, *50*, 2488–2490; e) N. Hasegawa, K. Shibata, V. Charra, S. Inoue, Y. Fukumoto, N. Chatani, *Tetrahedron* **2013**, *22*, 2266–4472; f) L. Troisi, C. Granito, S. Perrone, F. Rosato, *Tetrahedron Lett.* **2011**, *52*, 4330–4332; g) B. Gabriele, R. Mancuso, G. Salerno, L. Veltri, M. Costa, A. Dibenedetto, *ChemSusChem* **2011**, *4*, 1778–1786; h) B. Gabriele, R. Mancuso, G. Salerno, P. Plastina, *J. Org. Chem.* **2008**, *73*, 756–759; i) S.-M. Lu, H. Alper, *J. Am. Chem. Soc.* **2008**, *130*, 6451–6455.
- [7] For recent examples, see: a) L. Veltri, R. Mancuso, A. Altomare, B. Gabriele, *ChemCatChem* **2015**, *7*, 2206–2213; b) R. Mancuso, D. S. Raut, N. Della Cà, F. Fini, C. Carfagna, B. Gabriele, *ChemSusChem* **2015**, *8*, 2204–2211; c) A. Fini, M. Beltrani, R. Mancuso, B. Gabriele, C. Carfagna, *Adv. Synth. Catal.* **2015**, *357*, 177–184; d) B. Gabriele, L. Veltri, R. Mancuso, C. Carfagna, *Adv. Synth. Catal.* **2014**, *356*, 2547–2558; e) R. Mancuso, I. Zicarelli, D. Armentano, N. Marino, S. V. Giofrè, B. Gabriele, *J. Org. Chem.* **2014**, *79*, 3506–3518.
- [8] B. Gabriele, M. Costa, G. Salerno, G. P. Chiusoli, *J. Chem. Soc. Perkin Trans. 1* **1994**, 83–87.
- [9] For recent examples, see: a) L. Gatti, M. De Cesare, E. Ciusani, E. Corna, N. Arrighetti, D. Cominetti, L. Belvisi, D. Potenza, E. Moroni, F. Vasile, D. Lecis, D. Delia, V. Castiglioni, E. Scanziani, P. Seneci, N. Zaffaroni, P. Perego, *Mol. Pharm.* **2014**, *11*, 283–293; b) C. B. Bourguet, P.-L. Boulay, A. Claing, W. D. Lubell, *Bioorg. Med. Chem. Lett.* **2014**, *24*, 3361–3365.
- [10] The theoretical characterization of the transition states, which controlled the kinetics of different reaction steps, was outside the scope of the computational analysis carried out in this work, and will be reported in due course.
- [11] It is worth noting that noncovalent hydrogen bonding, H $\cdots\pi$, plays an important role in many chemical processes; for examples, see: a) C. Fonseca Guerra, F. M. Bickelhaupt, J. G. Snijders, E. J. Baerends, *J. Am. Chem. Soc.* **2000**, *122*, 4117–4128; b) S. J. Grabowski, T. L. Robinson, J. Leszczynski, *Chem. Phys. Lett.* **2004**, *386*, 44–48; c) S. J. Grabowski, W. A. Sokalski, J. Leszczynski, *J. Phys. Chem. A* **2005**, *109*, 4331–4341; d) S. J. Grabowski, W. A. Sokalski, *J. Phys. Org. Chem.* **2005**, *18*, 779–784; e) G. De Luca, A. Gugliuzza, E. Drioli, *J. Phys. Chem. B* **2009**, *113*, 5473–5477.
- [12] S.-M. Lu, H. Alper, *J. Am. Chem. Soc.* **2005**, *127*, 14776–14784.
- [13] M. Valiev, E. J. Bylaska, N. Govind, K. Kowalski, T. P. Straatsma, H. J. J. van Dam, D. Wang, J. Nieplocha, E. Apra, T. L. Windus, W. A. de Jong, *Comput. Phys. Commun.* **2010**, *181*, 1477–1489.

Received: November 4, 2015

Published online on January 28, 2016